Time-Dependent Quantum Mechanical Calculations on the Formation of Molecular Hydrogen on a Graphite Surface via an Eley−Rideal Mechanism†

Anthony J. H. M. Meijer,‡ Adam J. Farebrother,§ and David C. Clary*,||

Department of Chemistry, University College London, London WC1H 0AJ, United Kingdom

Andrew J. Fisher⊥

Department of Physics and Astronomy, University College London, London WC1E 6BT, United Kingdom

Received: October 18, 2000; In Final Form: December 14, 2000

The associative desorption of H_2 (v,j) on a graphite(0001) surface via an Eley−Rideal mechanism has been studied theoretically. In our calculations we used a time-dependent wave packet method treating three degrees of freedom quantum mechanically. A newly developed potential energy surface based on plane-wave density functional calculations was employed. In our 3D calculations we find less vibrational excitation for the product H_2 molecules than in calculations that used only two degrees of freedom. However, the product H_2 molecules are formed rotationally excited. This could have important implications for the chemistry of H_2 in the interstellar medium and the interpretation of astronomical data.

I. Introduction

Gas−surface reactions have long been of interest in physical chemistry. Most effort has been directed toward the study of dissociative adsorption, both experimentally (see, for example, refs 1−4) and theoretically (see, for example, refs 5−12). The inverse reaction of associative desorption has been studied much less, although there have been a number of theoretical[12−20] and experimental[2,21−24] studies.

Generally speaking, associative desorption can occur through two distinct mechanisms: the Langmuir−Hinshelwood (LH) mechanism and the Eley−Rideal (ER) mechanism.[25] In the LH mechanism the particles are adsorbed on a surface. They are thermalized to the surface temperature. Moreover, they diffuse across the surface, either via thermal diffusion or via tunneling. When two particles encounter each other, they can react. The energy released in the reaction is then either absorbed by the surface or used to desorb the product from the surface. In the ER mechanism only one particle is adsorbed on the surface and thermalized. It is also generally considered to be fixed on one site on the surface. A second particle subsequently comes from the gas phase and reacts directly with the adsorbed particle without first adsorbing on the surface. The excess energy again can be used to desorb the product. The LH mechanism has been studied more extensively than the ER mechanism, because of its importance in catalysis. The ER mechanism was long considered to be fairly unimportant. However, in the last few years reactions have been found where the ER mechanism plays an important role.[2,21−24,26−29] Theoretically, most research has been done on catalytic systems,[13−19] although some astrophysically relevant systems have also been studied.[30,31] Obviously, combinations of the LH and ER reaction mechanisms are also possible, see, for example, the hot-atom (HA) mechanism, where the second particle does adsorb on the surface. However, it does not thermalize and reacts after only a short time on the surface.

The motivation for studying the formation of H_2 on a graphite surface via an Eley−Rideal mechanism lies mainly in astrophysics. The hydrogen molecule is the most abundant molecule in interstellar space, especially in dense molecular clouds. H_2 plays an important role in the cooling of these molecular clouds. This allows the clouds to continue their gravitational collapse leading to the formation of stars. H_2 is also a very important molecule in most networks of chemical reactions in the interstellar medium (ISM).

The formation mechanism of H_2 from H atoms in the ISM has been the subject of much debate (see, for example, refs 32−35). Three-body collisions are an unlikely mechanism as they are very rare in the ISM, because of the low concentration of atoms. Another option would be direct radiative association of two hydrogen atoms. However, this reaction is strongly forbidden[32] and therefore unlikely to be important. A third possibility would be the reaction of H^- with H leading to H_2 and an electron. This reaction is considered to be important in the early Universe. However, its reaction rate is not high enough to explain the observed concentration of H_2 molecules, especially in molecular clouds.[32]

The generally accepted mechanism of the formation of H_2 in the ISM is via associative desorption on interstellar dust grains.[32,33,36] This mechanism is the only one proposed for which reaction rates can be calculated that are high enough to explain the H_2 abundance in the ISM, despite the low temperatures of the dust particles (≈10 K) and the gas-phase atoms (10−100 K). The precise form of the interstellar dust is not known. However, there is evidence from analysis of meteorites that dust particles can be coated in carbon (see, for example, refs 37−39). There is also evidence for the existence of graphite in dust grains through the observed extinction "hump" at 217.5 nm (see, for example, refs. 40−42). Therefore, most models include amorphous carbon (for an overview see ref 43). The precise

† Part of the special issue "Aron Kuppermann Festschrift".

* Author to whom correspondence should be addressed.
‡ E-mail: a.meijer@ucl.ac.uk.
§ E-mail: a.farebrother@ucl.ac.uk.
|| E-mail: d.c.clary@ucl.ac.uk.
⊥ E-mail: andrew.fisher@ucl.ac.uk.

10.1021/jp003839+ CCC: $20.00
Published on Web 03/15/2001

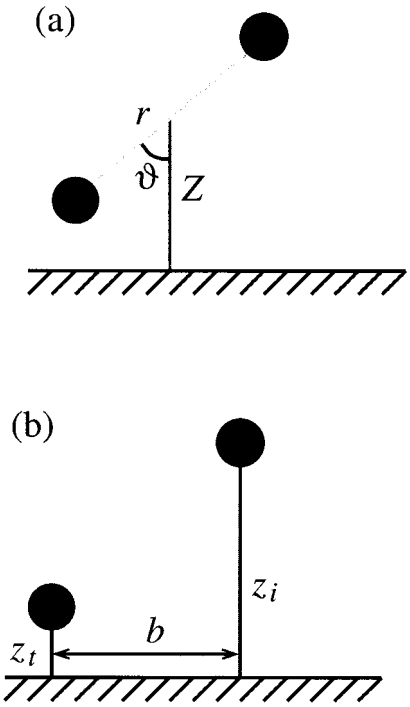

Figure 1. (a) Product coordinates and (b) reactant coordinates.

reaction mechanism is also not known. Both the LH[44] and ER mechanisms have been proposed.[45] The formation of H_2 on graphite has mainly been studied experimentally.[44,46−50] There have been a small number of prior theoretical studies of this reaction (see, for example, refs 30,31,51). Other related systems have been studied as well.[52,53]

The goal of the present study is to perform calculations on the H_2 formation on graphite through the Eley−Rideal mechanism under conditions that are relevant to the ISM. For this we use a time-dependent wave packet method and a newly developed potential based on a LEPS formulation[54] and on plane-wave density functional calculations.[31] We calculate the probabilities of producing H_2 in particular rotational and vibrational states. The calculations are being done to complement experiments currently underway in our laboratory.[55]

The organization of the paper is as follows. In Section II we discuss the theory and some computational details. In Section III we discuss our results, and in Section IV we present our conclusions.

II. Theory and Computational Details

A. Coordinate System, Flat Surface Model, and Basis Functions. We start by introducing some notation. The Cartesian coordinates of the incident H atom are given by $\mathbf{x}_i = (x_i, y_i, z_i)$. The coordinates of the adsorbed (target) H atom are given by $\mathbf{x}_t = (x_t, y_t, z_t)$. We find it more convenient to transform to a relative position vector $\mathbf{r} = \mathbf{x}_t - \mathbf{x}_i$ and center of mass position vector $\mathbf{X} = (m_i\mathbf{x}_i + m_t\mathbf{x}_t)/M$, where $M = m_i + m_t$, the total mass of the resultant molecule. $\mathbf{r}$ is most conveniently expressed in polar coordinates, $\mathbf{r} = \mathbf{r}(r,\vartheta,\varphi)$, where r is the length of $\mathbf{r}$, ϑ is the polar angle, and φ is the azimuthal angle. $\mathbf{X}$ will be used in Cartesian coordinates, $\mathbf{X} = \mathbf{X}(X,Y,Z)$, where X, Y, and Z are the position of the center-of-mass of the molecule above the surface.

In our calculations we use a fixed surface, i.e., we neglect the influence of surface phonons on the reaction probabilities. This assumption is probably not severe for studying the Eley−Rideal reaction of H on graphite, because of the mass difference between hydrogen and graphite. Moreover, our calculations will be done within the flat surface approximation (FSA).[13−16] This means that we also neglect the corrugation of the graphite surface. Consequently, in our model the potential energy surface (PES) is invariant under translation of the center-of-mass of the molecule over the surface. The FSA also introduces an axial symmetry to the potential for rotations parallel to the surface, meaning that the azimuthal quantum number m associated with this motion will be conserved. Thus the PES, V, will only be a function of Z, r, and ϑ, which are plotted in Figure 1a for clarification. We expand the wave function as a function of these coordinates and m. We use a sinc-DVR (discrete variable representation)[56] with "wrapped" basis functions,[57] $\phi_k^-(Z)$ and $\phi_i^-(r)$, for the Z and r coordinates, respectively. Note that we can use the wrapped sinc-DVR for Z, since it has a domain of $[0,\infty]$ just like r. We use a symmetry-adapted Gauss−Legendre DVR[58−60] with basis functions $\psi_1(\vartheta)$ for ϑ. This DVR is used, because we can use the permutation-inversion symmetry of the resultant H_2 molecule to select only odd or even rotational states, corresponding to o-H_2 or p-H_2, respectively. Consequently, we need only half of the Gauss−Legendre DVR points.[59] This results in the following expansion for the wave function, $\Psi^m(Z,r,\vartheta,\varphi;t)$:

$$\Psi^m(Z,r,\vartheta,\varphi;t) = \sum_k^{N_Z}\sum_i^{N_r}\sum_l^{N_\vartheta} c_{kil}^m(t)\phi_k^-(Z)\phi_i^-(r)\psi_l(\vartheta)\frac{1}{\sqrt{2\pi}}e^{im\varphi} \quad (1)$$

where the factor $1/\sqrt{2\pi}$ arises from the normalization of $e^{im\varphi}$. Throughout this paper we will use $\Psi^m(Z,r,\vartheta,\varphi;t)$ instead of the proper wave function $\Phi^m(Z,r,\vartheta,\varphi;t)$. The two are related as $\Phi^m(Z,r,\vartheta,\varphi;t) = \Psi^m(Z,r,\vartheta,\varphi;t)/r$. This ensures that the volume element of the wave function is unity and that the Hamiltonian can be written in pseudo-Cartesian form as in eq 5.

B. Potential. In a previous publication we presented the results of the calculation of a potential energy surface (PES) for the H + H−graphite system.[31] We chose to model the graphite (0001) surface as a monolayer with periodic boundary conditions and 18 carbon atoms per supercell. The electronic structure was treated within the generalized gradient approximation (GGA) to density functional theory using the projector-augmented plane wave (PAW) method.[61−63] The exchange correlation energy was described using the Becke-Perdew 86 functional.[64−66] For more details see ref 31. These electronic structure calculations were restricted to a collinear (2D) collision geometry, because using the GGA-PAW method to calculate a full 3D potential would be too time-consuming with the computer hardware currently available to us. Therefore, we followed a different approach to obtain a 3D potential energy surface. This approach is similar to the one followed by Kalyanaraman, Lemoine, and Jackson in studies of H/D impinging on H/D adsorbed on Cu(111).[16] Our procedure is as follows.

First, we use a spline-fit to get a global representation of the potential using the GGA points of ref 31 and the asymptotic extension of the potential. We subsequently scaled this potential to obtain the correct vibrational energies for H_2, i.e., we replaced the spline-fitted potential $V(z_i,z_t)$ by $s_1V(s_2z_i,s_2z_t)$, where s_1 equals 0.807 and s_2 equals 1.365. To this potential we fitted a model potential of the LEPS (London, Eyring, Polyani, and Sato) form[54] using an eight-parameter least-squares fit, which is defined as

$$V(Z,r,\vartheta) = V(r,z_i,z_t) = U_a(z_i) + U_a(z_t) + U_b(r) - \{[Q_a(z_i) + Q_a(z_t)]^2 + Q_b^2(r) - [Q_a(z_i) + Q_a(z_t)]Q_b(r)\}^{1/2} \quad (2)$$

where

$$U_\lambda(x) = \frac{D_\lambda}{4(1+S_\lambda)}[(3+S_\lambda)e^{-2\alpha_\lambda(x-x_\lambda^{(0)})} - (2+6S_\lambda)e^{\alpha_\lambda(x-x_\lambda^{(0)})}] \quad (3)$$

and

$$Q_\lambda(x) = \frac{D_\lambda}{4(1+S_\lambda)}[(1+3S_\lambda)e^{-2\alpha_\lambda(x-x_\lambda^{(0)})} - (6+2S_\lambda)e^{\alpha_\lambda(x-x_\lambda^{(0)})}] \quad (4)$$

In eqs 3 and 4, $\lambda = a$ (atom−surface interaction) or $\lambda = b$ (molecular interaction). There exists a simple geometric transformation between the (Z,r,ϑ) and the (r,z_i,z_t) coordinates.

After fitting the LEPS potential to the ab initio data, we reoptimized the molecular well depth D_b, the molecular potential strength α_b, and the molecular equilibrium distance $x_b^{(0)}$ to get better agreement with experimental rovibrational energies for H_2. D_b was shifted to 4.75 eV.[30,67] $x_b^{(0)}$ was set to the experimental value for the equilibrium distance, 1.40 bohr.[68] Last, α_b was put at an optimal value for agreement with experimental rovibrational energies. The complete set of parameters is given in Table 1. This results in a dissociation energy for H_2 of 36099.2 cm^{-1}, close to the experimental energy of 36118.3 cm^{-1}.[68] The agreement with the experimental vibrational energies is also quite good as is clear from a number of representative examples given in Table 2, especially for rotational excitation. With this choice of parameters the exothermicity of the potential is 2.75 eV. The binding energy of H on graphite is 1.72 eV, about 50% of the binding energy of the bond strength of CH at 298 K.[69] It is slightly larger than the possible values for the C−H bond strength given in ref 46. Similar methods of obtaining a 3D potential from a 2D potential without additional electronic structure calculations have been widely used in gas-phase scattering. Also in gas−surface scattering they have been shown to give a good fit for the LEPS parameters.[70]

C. Hamiltonian and Propagation. With the current choice of our coordinate system, we can write the Hamiltonian as follows:

$$\hat{H} = -\frac{\hbar^2}{2M}\frac{\partial^2}{\partial Z^2} - \frac{\hbar^2}{2\mu}\frac{\partial^2}{\partial r^2} + \frac{\hat{j}^2}{2\mu r^2} + V(Z,r,\vartheta) \quad (5)$$

where μ is the reduced mass of the H_2 molecule. Note that this Hamiltonian can be seen as the FSA form of the Hamiltonian commonly used to study dissociative adsorption.[7,8] If we use eqs 1 and 5 in combination with the time-dependent Schrödinger equation, we obtain the following equations-of-motion:

$$i\hbar\frac{\partial c_{kil}^m(t)}{\partial t} = -\sum_{k'} T_{kk'}^Z c_{k'il}^m(t) - \sum_{i'} T_{ii'}^r c_{ki'l}^m(t) + \sum_{l'} T_{ll'}^\vartheta(r_i) c_{kil'}^m(t) + V(Z_k,r_i,\vartheta_l)c_{kil}^m(t) \quad (6)$$

The relationships $T_{kk'}^Z = \hbar^2/2M\langle\phi_k^-(Z)|\partial^2/\partial Z^2|\phi_{k'}^-(Z)\rangle$ and $T_{ii'}^r = \hbar^2/2\mu\langle\phi_i^-(r)|\partial^2/\partial r^2|\ \phi_{i'}^-(r)\rangle$ can be evaluated analytically.[56,57,71] The evaluation of $T_{ll'}^\vartheta(r_i) = \langle\psi_l(\vartheta)|\hat{j}^2/2\mu r_i^2|\psi_{l'}(\vartheta)\rangle$ is less straightforward. It is advantageous for our calculations to restrict the range of eigenvalues for **H**, the matrix representation of $\hat{H}$. Therefore, we use a cutoff on the values of $T_{ll'}^\vartheta(r_i)$. This cutoff is most easily and systematically applied in a finite basis representation (FBR). However, handling the angular coordinate with an FBR would require the storage of a large matrix of integrals of the potential over the angular coordinate, whereas in a DVR this matrix is diagonal. Thus, we perform the application of the scattering, vibrational, and potential terms of the Hamiltonian to the wave function in the DVR. For the rotational term, we transform the wave function to an FBR, apply the rotational operator, and transform back to the DVR.[72] To make this FBR-DVR transformation as efficient as possible we implemented it as a matrix−matrix multiplication instead of a matrix−vector multiplication (see ref 72 for more details).

TABLE 1: Parameters for LEPS Potential

parameters	value	unit
D_a	0.06784450	a.u.
S_a	−0.310216	
α_a	1.10999	$a.u.^{-1}$
$x_a^{(0)}$	1.76486	a.u.
D_b	0.174559	a.u.
S_b	0.593297	
α_b	1.045838	$a.u.^{-1}$
$x_b^{(0)}$	1.40547	a.u.

TABLE 2: H_2 Rovibrational Energies: Theory vs Experiment

(v,j)	calcd. (cm^{-1})	expt. (cm^{-1})
(0,0)	0.000	0.000
(0,1)	118.48	118.495
(0,2)	354.37	354.397
(1,0)	4213.82	4162.047
(1,1)	4327.43	4274.628
(1,2)	4553.53	4498.739
(2,0)	8166.35	8088.667
(2,1)	8274.83	8195.465
(3,0)	11857.62	11784.787
(4,0)	15287.62	15253.415
(5,0)	18456.38	18495.536
(6,0)	21363.94	21509.850

To propagate the wave function in time, we use the real wave packet propagation method of Gray and Balint-Kurti.[73] Similar methods have been developed by others.[74−77] This method is based on three ideas. First, we can infer reaction probabilities from only the real part q of a wave packet Ψ.[78] Second, we can obtain correct reaction probabilities from the propagation of the wave packet using a modified Schrödinger equation, where $\hat{H}$ is replaced by a function of itself, $f(\hat{H})$. Third, we can choose $f(\hat{H})$ so that the following Chebychev recursion relation holds:

$$q_{\kappa+1} = \mathbf{A}(-\mathbf{A}q_{\kappa-1} + 2\mathbf{H}_s q_\kappa) \quad (7)$$

where $\mathbf{H}_s = a_s\mathbf{H} + b_s$. a_s and b_s are chosen such that the eigenvalues of **H** lie between −1 and 1. The damping matrix **A** ensures that the wave packet is absorbed at the edge of the grid to avoid unphysical reflections.[72,79,80]

D. Initial States and Final Analysis. We start our calculations with a Gaussian distribution in z_i of the form

$$G(z_i) = \frac{1}{\sqrt[4]{2\pi\beta}}e^{-ik_0z_i}e^{-(z_i-z_0)^2/4\beta} \quad (8)$$

where z_0 is the center of the initial wave packet and k_0 is the initial momentum perpendicular to the surface. The atom on

the surface is considered to be in the lowest vibrational eigenstate, $v_0(z_t)$, which has energy ϵ_t. In this article we are concerned only with a perpendicular approach to the surface (i.e., $m = 0$). Therefore, we can write the initial wave packet as[16]

$$Y^{m=0}(z_i,z_t,b) = G(z_i)v_0(z_t)F(b) \tag{9}$$

where b is the impact parameter and $F(b)$ defines the radial part of the wave packet. A graphical representation of these reactant coordinates is given in Figure 1b. $F(b)$ has the following form

$$F(b) = \sqrt{\frac{2\pi}{A_b}}\begin{cases}1 & b < b_{\max}\\ e^{-[(b-b_{\max})\gamma]^2} & b > b_{\max}\end{cases} \tag{10}$$

where $b_{\max}$ is chosen to be larger than the maximum reactive impact parameter. $F(b)$ normalizes the radial part of the wave packet. A_b normalizes $F(b)$ and is given as

$$A_b = \pi b_{\max}^2 + \frac{\pi}{2\gamma^2} + \sqrt{\frac{b_{\max}^2}{2\pi\gamma^2}} \tag{11}$$

$F(b)$ is not an eigenstate of the radial Hamiltonian, so there is a possibility of a dependence of the final result on z_0, because of spreading and distortion of the wave packet. We removed this difficulty by making the initial wave packet quite diffuse, choosing $\gamma = 0.2$ bohr^{-1}, $b_{\max} = 5$ bohr, and $z_0 = 14$ bohr.

At this point we could have used the wave packet of eq 9 in a wave packet calculation. Instead, we have chosen to transform Y to the (Z,r,ϑ) grid and perform the calculation using the Hamiltonian of eq 5. The reasoning behind this is straightforward. At one point in our calculations we will have to do a transformation to the (Z,r,ϑ) coordinates to obtain reaction probabilities as a function of the rovibrational state of the H_2 molecule. This involves interpolating the wave function from the (z_i,z_t,b) grid on the (Z,r,ϑ) grid. This is much easier to accomplish and with greater precision with the smooth localized initial wave packet than with the heavily structured, spread out final wave packet. Since the value of the wave function has to be independent of the coordinate representation, the following holds:

$$Y^{m=0}(z_i,z_t,b) = \Phi^{m=0}(Z,r,\vartheta;\, t=0) = \Psi^{m=0}(Z,r,\vartheta;\, t=0)/r \tag{12}$$

where (z_i,z_t,b) and (Z,r,ϑ) are related by a geometric transformation. Thus, in setting up our initial wave packet, we cycle through our (Z,r,ϑ) grid, generate the corresponding (z_i,z_t,b), and interpolate $Y^{m=0}$ at that point. Actually, only $v_0(z_t)$ needs to be interpolated, since $G(z_i)$ and $F(b)$ are known analytically.

The final analysis is done using a flux method.[79,81,82] The reaction probability as a function of total energy, $P(E)$, is defined as

$$P(E) = \frac{\hbar}{\mu}\mathrm{Im}\langle\Psi^+(E)|\hat{F}(Z_s)|\Psi^+(E)\rangle \tag{13}$$

with μ the reduced mass of H_2 and $\hat{F}(Z_s)$ the flux operator for the flux through a surface at Z_s. $\Psi^+(E)$ is the scattering wave function. For more details, see refs 79, 81, 82. The state-resolved reaction probability, $P_{vj}(E)$, is simply obtained by introducing the projection operator $\hat{P}_{vj}$, which is defined as[82]

$$\hat{P}_{vj} = \frac{1}{P(E)}|v_v(r)Y_{jm}(\vartheta)\rangle\langle Y_{jm}(\vartheta)v_v(r)| \tag{14}$$

which projects $\Psi^+(E)$ onto the rovibrational eigenfunction labeled by v and j. Division by $P(E)$ ensures that the state selected reaction probabilities add up to one. The nonreaction probability can be defined in a similar way to $P(E)$, only in this case the surface lies at r_s. The fact that the probabilities always sum to one for a converged calculation is a diagnostic on the quality of the calculation. Note that we plot $P(E_i)$ in Section III, where E_i is the initial translational energy, defined as $E - \epsilon_t$.

Since we deal only with perpendicular collisions within the FSA, m will be zero (cartwheel motion). Therefore, we will omit the superscript m for economy of notation.

E. Computational Details. We calculate the initial wave packet and propagate it forward in time using the real propagation method of Gray and Balint-Kurti.[73] To facilitate the evaluation of $\mathbf{H}_s q_k$ (see eq 7) we use the sorting algorithm of Groenenboom and Colbert[57] and the point selection scheme of Meijer and Goldfield.[79] After N_t steps we calculate the derivative of the wave function at r_s and Z_s. These are stored on disk together with a cut of the wave packet at r_s and Z_s. After the propagation we use these vectors to calculate $P(E)$.

The most important parameters for the propagation are given in Table 3. Where a symbol has not been mentioned in the article so far, a short explanation is given. A complete set of parameters is available on request.

III. Results and Discussion

In this section we will discuss the results of our calculations. First, we will discuss the results for a collinear collision, i.e., 2D calculations in which the product H_2 molecule is nonrotating. This allows us to make a direct comparison with time-independent calculations using the method of ref 31. Subsequently, we discuss our 3D calculations. We also discuss the implications of our calculations for astronomical models.

A. 2D Calculations. For our 2D calculations we used the same parameters as for our 3D calculations (see Table 1). We only needed 17 000 propagation steps (≈870 fs) instead of 30 000. Thus, the reaction in the 2D approximation finishes twice as fast as the reaction in the 3D approximation.

In Figure 2 we plotted the reaction probabilities as a function of vibrational quantum number from our time-dependent (TD) calculations together with reaction probabilities generated with the time-independent (TI) program that was used to generate the results of ref 31. As is clear from the graph the two calculations match up very well, especially given that the methods are so dissimilar. The agreement deteriorates at low

TABLE 3: Parameters for Time-Dependent Wave Packet Calculation

name	description	value
$t_{\max}$	maximum propagation time	30 000 steps
$Z_{\min}$	minimum value for Z	0 bohr
$Z_{\max}$	maximum value for Z	20.0 bohr
N_Z	number of DVR functions in Z	200
Z_s	analysis distance for Z	9.45 bohr
Z_{abs}	start absorption region in Z	10.00 bohr
$r_{\min}$	minimum value for r	0 bohr
$r_{\max}$	maximum value for r	30.0 bohr
N_r	number of DVR functions in r	300
r_s	analysis distance for r	21.42 bohr
r_{abs}	start absorption region in r	22.00 bohr
$j_{\max}$	maximum value for j	220
N_t	see Section II E	8

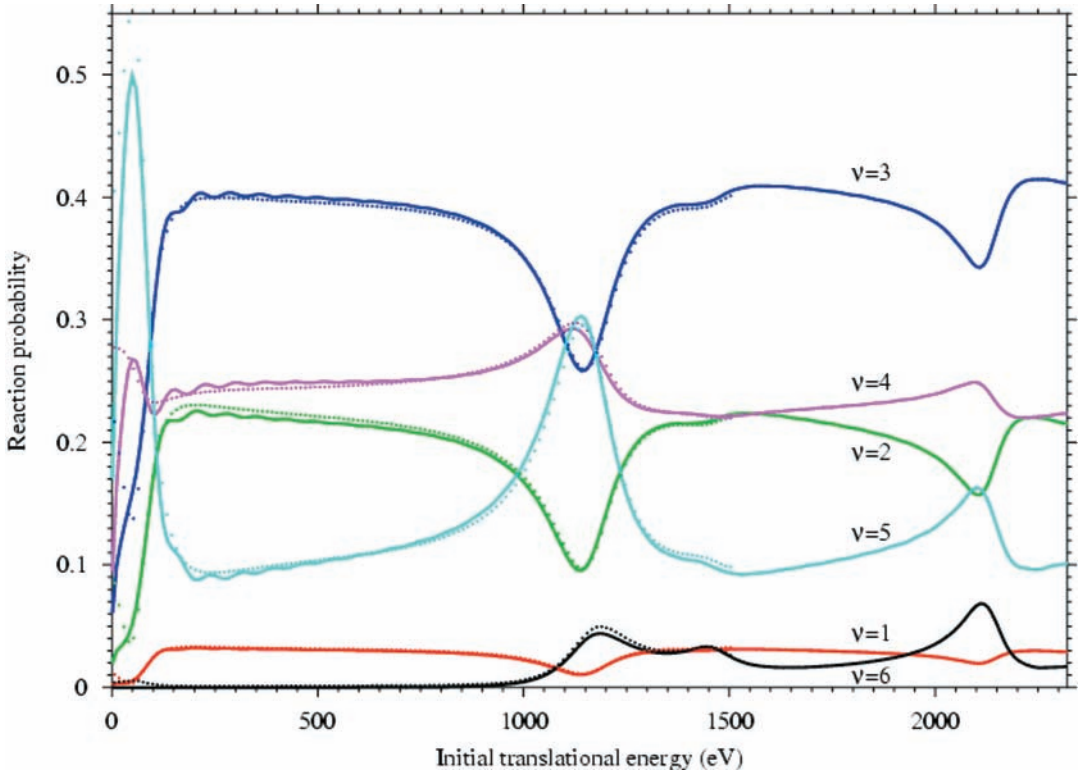

Figure 2. 2D state-resolved reaction probabilities as a function of initial translational energy: time-dependent calculations (solid lines) vs time-independent calculations (dotted lines).

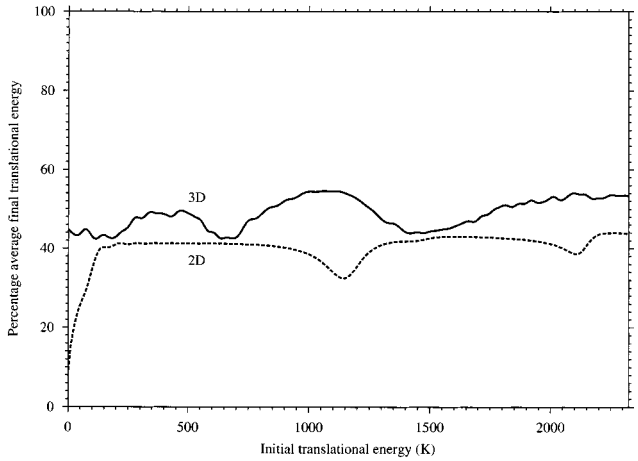

Figure 3. Average final translational energy of H_2 as a percentage of the total energy as a function of the initial translational energy of the H atom.

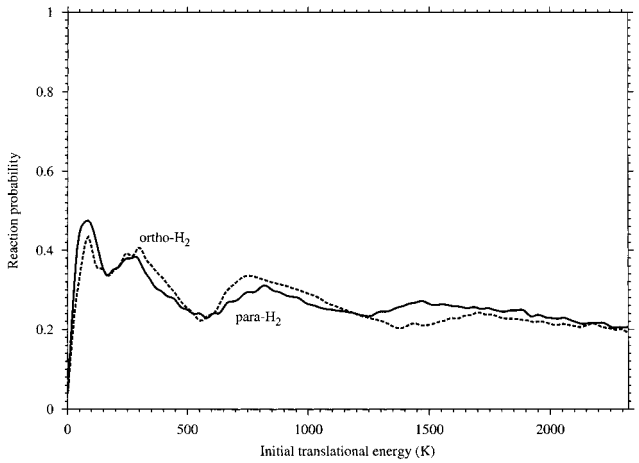

Figure 4. Total reaction probability for producing *o*-H_2 and *p*-H_2 as a function of the initial translational energy of H atom for 2D and 3D calculations.

initial translational energy. This is to be expected. Parts of the wave packet with low initial translational energy will travel very slowly to the reaction region. Therefore, it will take longer to get these energies resolved. Moreover, low initial translational energy means long de Broglie wavelengths, which are represented worse on a finite grid than shorter de Broglie wavelengths. The good agreement between the TD and TI calculations allows us to put a lower limit on the translational energies from the TD calculations that can be trusted. Based on this figure we determine that our calculations can be trusted down to approximately 100 K (=0.0086 eV). This means that we can extract information from our calculations at a temperature relevant to the interstellar medium, since most dense molecular clouds are at a temperature between 10 and 100 K.

In Figure 3 we plotted the ratio of the average final translational energy to the total energy of the product H_2 molecule. As is clear from the figure the molecule exits the surface translationally very hot. This can be significant in the interstellar medium, since that translational energy can be used to overcome reaction barriers in subsequent reactions with other molecules or it can be transferred to other molecules/atoms via inelastic collisions. Interestingly, the resonance structure which is so clear in the reaction probabilities in Figure 2 survives into the ratio plotted in Figure 3. We also plotted the 3D average kinetic energy in Figure 3, but will discuss this when we compare the 2D and 3D calculations.

B. 3D Calculations. In Figure 4 we show the total reaction probability for the *o*-H_2 and the *p*-H_2 formation for our 3D calculations. As is clear from the figure the reaction probability drops in value compared to the 2D calculations, where it was very close to unity. The reaction probability for *o*-H_2 and *p*-H_2 are very similar. Therefore, we will present our results for all

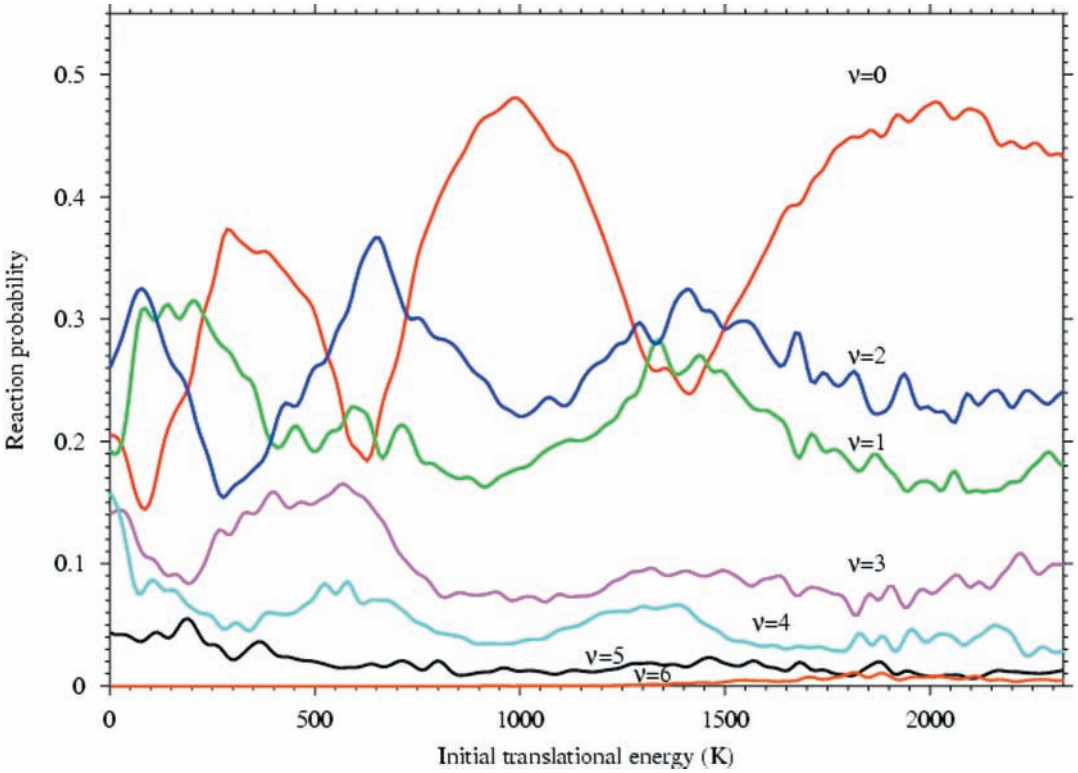

Figure 5. Reaction probabilities for producing H_2 summed over rotational states, $\bar{P}_v(E_i)$ as a function of initial translational energy of the H atom.

rotational states at the same time without separately discussing *o*-H_2 and *p*-H_2. The reaction probabilities show some dependence on initial translational energy, dropping from 0.42 at 100 K to 0.2 at 2300 K.

Before we continue to discuss the state-selected reaction probabilities for the 3D calculations, we discuss the differences between the 2D and the 3D calculations. Thus, we examine the ratio between the average final kinetic energy of the product molecule and the total energy. This is plotted in Figure 3 for both 2D and 3D calculations. As is clear from comparing the two curves in Figure 3, the product molecules in the 3D calculations are translationally hotter than the molecules in the 2D calculations. Moreover, the 3D curve shows more structure and the resonance features lie at different initial translational energies. This is an indication that the dynamics of the 3D calculation are different from those of the 2D calculations. This becomes clearer when we compare the 2D reaction probabilities of Figure 2 with the reduced reaction probabilities $\bar{P}_v(E_i) = \sum_j P_{vj}(E_i)$ for the 3D calculations as a function of initial translational energy (Figure 5). The first thing that is clear from Figure 5 is that instead of a vibrationally excited H_2 molecule in $v \geq 2$ as in the 2D calculations, we find H_2 molecules with $v \leq 2$ for the 3D calculations. Moreover, the $v = 0$ state has the highest population. Another difference is that the resonance features, which are so clear in Figure 2, are obscured in Figure 5. Moreover, they occur at different initial translational energies.

The H + H−graphite reaction is highly exothermic. Therefore, many product states are populated. This makes it confusing to present our 3D results in the manner of Figure 2. Thus we have decided to present the 3D results at a number of representative energies. These energies are 98 K (= 8.45 meV), 201 K (= 17.32 meV), 296 K (= 25.51 meV), 504 K (= 43.43 meV), 627 K (= 54.03 meV), 988 K (= 85.14 meV), 1425 K (= 0.1228 eV), and 1976 K (= 0.1703 eV). The first two energies are interesting from an astrophysical point of view. The other energies lie on maxima or minima in the $v = 0$ reduced reaction probability, except 504 K, which lies on a maximum in the $v = 3$ reduced reaction probability. The state selected reaction probabilities are given in Figure 6. The reaction probabilities show quite dramatic changes as a function of initial translational energy, as can be expected from Figure 5. In Figure 6, panel (a), there are three sharp peaks at $v = 1$, $j = 16$, $v = 2$, $j = 13$, and $v = 4$, $j = 9$. Looking at panel (b) we see that only the peak at $v = 1$, $j = 16$ remains. We attribute these features to resonances in the interaction region. The nature of these resonances cannot be deduced from the present calculations. However, we suspect it to be a resonance to form an excited H−graphite bond, which subsequently dissociates to a specific rovibrational state of H_2. We see the same type of resonances appear at all other energies in Figure 6. Note that for the entire energy range covered by Figure 6 the highest rotational quantum number is $j = 20$, independent of initial translational energy over this energy range. This indicates a dynamical limit for energy transfer between translational and rotational energy for this reaction.

In general, at all energies the product H_2 is highly rotationally excited. This becomes even clearer when we plot the reduced reaction probability $\tilde{P}_j(E_i) = \sum_v P_{vj}(E_i)$ versus initial translational energy in Figure 7. Since the highest rotational quantum number, j_{max}, is 20, there would be 21 curves for $\tilde{P}_j(E_i)$. Therefore, we have chosen to plot $\tilde{P}_j(E_i)$ only at the energies used in Figure 6. For each energy we see a bimodal distribution of $\tilde{P}_j(E_i)$ to some extent with maxima near $j = 8$ and $j = 14$. The clearest examples are for 988 and 1425 K. A similar effect was found by Jackson and Persson in their flat-surface calculations on the surface-catalyzed formation of H_2 from a Cu(001) surface via the Eley−Rideal mechanism.[14] They concluded from comparing their calculations to quasi-classical trajectory (QCT) calculations on the same potential energy surface that it was probably due to an interference effect in the quantum dynamics calculations, since it did not show up in the QCT calculations.

To investigate whether the resonances of Figure 6 might be

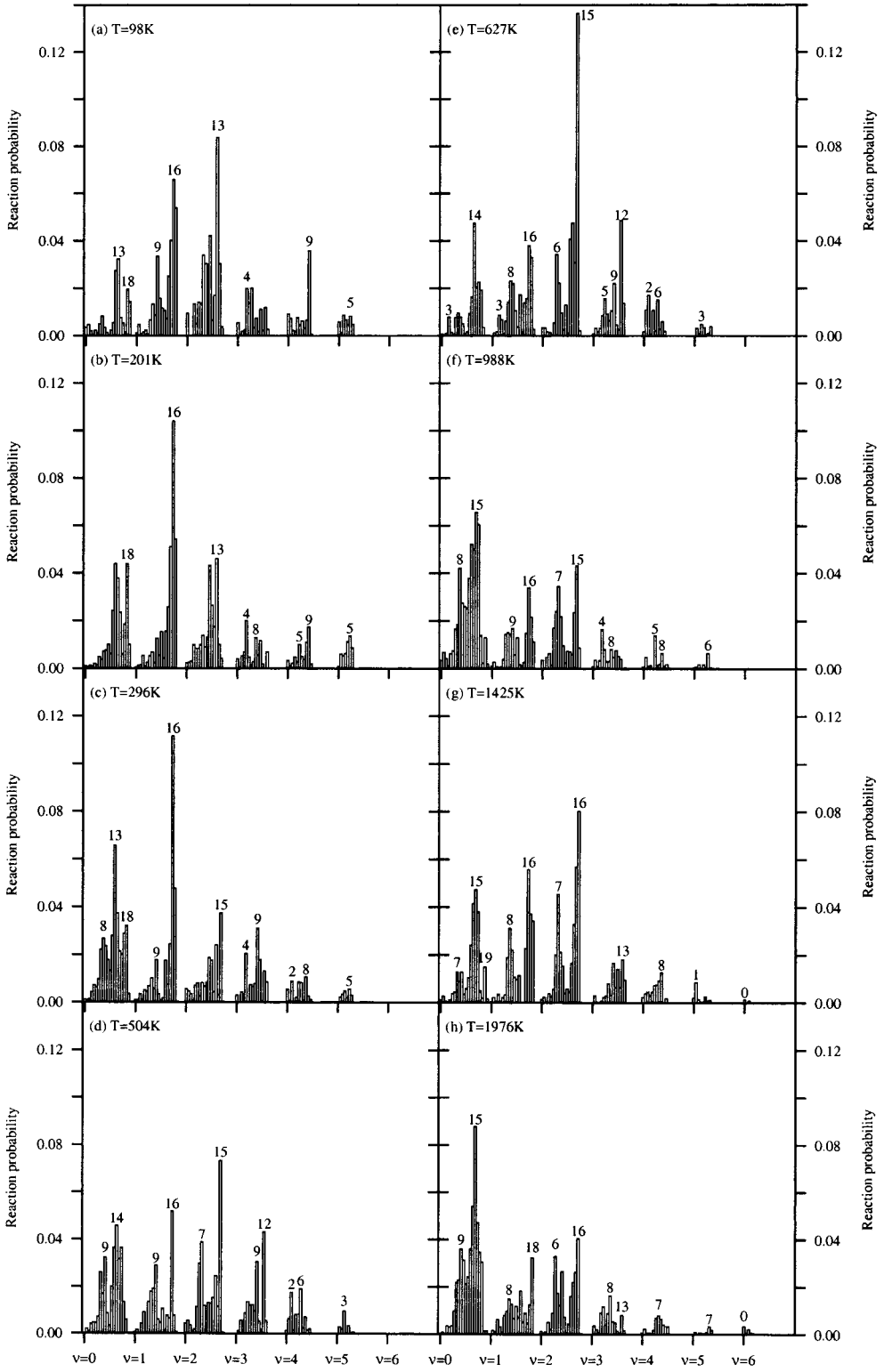

Figure 6. Reaction probabilities for producing H_2 in specified (v,j) state at initial translational energies of the H atom of 98 K, 201 K, 296 K, 504 K, 627 K, 988 K, 1425 K, and 1976 K.

caused by an excitation of one specific H-surface mode, we plotted the reaction probabilities as a function of final rovibrational energy for the eight energies used in Figure 8. As can be expected, we see very little population of low-energy rovibrational states for the energies where $\bar{P}_{v=0}(E_i)$ is at a minimum (98 K, 628 K, and 1425 K). However, there appears to be no clustering of high reaction probabilities at certain final rovibrational energies and between initial translational energies. The distribution of reaction probabilities over final rovibrational energies appears only to be weakly dependent on the initial translational energy. From Figure 8 it is clear that the product H_2 molecule is formed with significant translational energy. The minimum final translational energy is 1410 cm^{-1} (2029 K) at an initial translational energy of 1976 K. For the states with the largest reaction probability this is more, e.g., at 98 K it is approximately 5000 cm^{-1} (approximately 7200 K).

The graphite-catalyzed formation of H_2 in interstellar space via an Eley−Rideal mechanism has been studied previously by

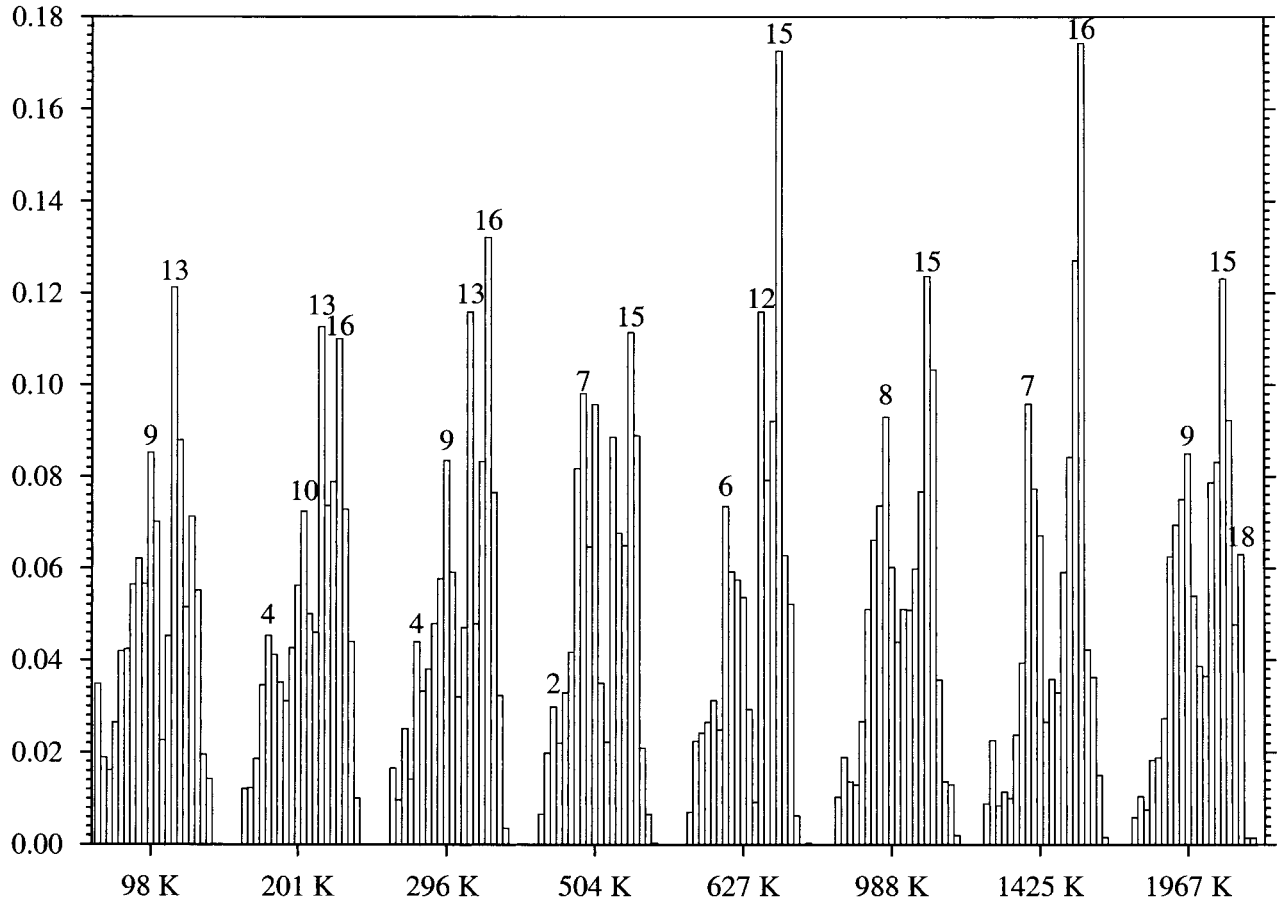

Figure 7. Reaction probabilities for producing H_2 summed over vibrational states, $\tilde{P}_J(E_i)$, at initial translational energies of the H atom of 98 K, 201 K, 296 K, 504 K, 627 K, 988 K, 1425 K, and 1976 K.

Parneix and Bréchignac (PB).[30] In their study they used classical mechanics and a semiempirical potential based (partly) on MINDO/3 calculations. They also used an atom−atom potential in their calculations, although the mathematical form of their potential is different from ours. The main difference between the two potentials is that in their case the potential has a barrier in the entrance channel. This significantly alters the dynamics of the H + H−graphite system and it is therefore not surprising that our results are at variance with the PB results. For instance, they find a statistical distribution for the reduced reaction probability, $\bar{P}_v(E_i)$, which is clearly not the case for our calculations. Furthermore, they do not find a bimodal distribution for $\tilde{P}_J(E_i)$. However, this could also be due to the fact that they use classical mechanics instead of quantum dynamics, as was mentioned earlier. In both calculations the product H_2 molecule is translationally hot when formed. In the PB calculations the average final translational energy is about 50% of the total energy, as in our calculations. However, in their case it is constant as a function of initial translational energy with no resonance structure present.

If H_2 in the ISM is indeed formed translationally hot and rovibrationally excited, then that has a number of significant consequences. First of all, reactions of vibrationally excited H_2 can have much larger reaction rates than those of H_2 in the vibrational ground state. Moreover, the large amount of translational energy released during the Eley−Rideal reaction means that also some endothermic reactions might become possible. The rovibrational excitation and large kinetic energy release together might mean that reactions such as, for example, $C^+ + H_2$ and $O(^3P) + H_2$ might be possible under conditions in the ISM. Second, the presence of highly vibrationally excited H_2 molecules ($v \geq 4$) might mean that direct ionization of H_2 or charge-exchange with H^+ become feasible, leading to H_2^+. H_2^+ can subsequently react to form H_3^+, a very important molecule in the ISM. Third, the large kinetic energy release can lead to localized heating of the molecular cloud through inelastic scattering processes.

IV. Conclusions

We have performed time-dependent quantum mechanical calculations on the surface-catalyzed formation of H_2 on a graphite(0001) surface via the Eley−Rideal reaction mechanism. This process is a possible pathway for the formation of H_2 in dense molecular interstellar clouds. H_2 plays an important role in these clouds as a cooling agent in their collapse leading to the formation of stars. Moreover, H_2 forms the starting point of many reactions in interstellar space.

In our calculations we neglect the corrugation and the phonons of the graphite surface, reducing the number of degrees-of-freedom to be treated to three. We have developed a 3D semiempirical potential energy surface for this reactive system based on earlier DFT/GGA calculations.[31] This potential has the form of a LEPS potential and was used in 2D (collinear) calculations and in 3D calculations.

The 2D calculations were used to check our time-dependent calculations against time-independent calculations. This gives us an idea of the accuracy of our calculations, especially at low translational energies where convergence of the time-dependent calculations is a problem, because of long propagation times

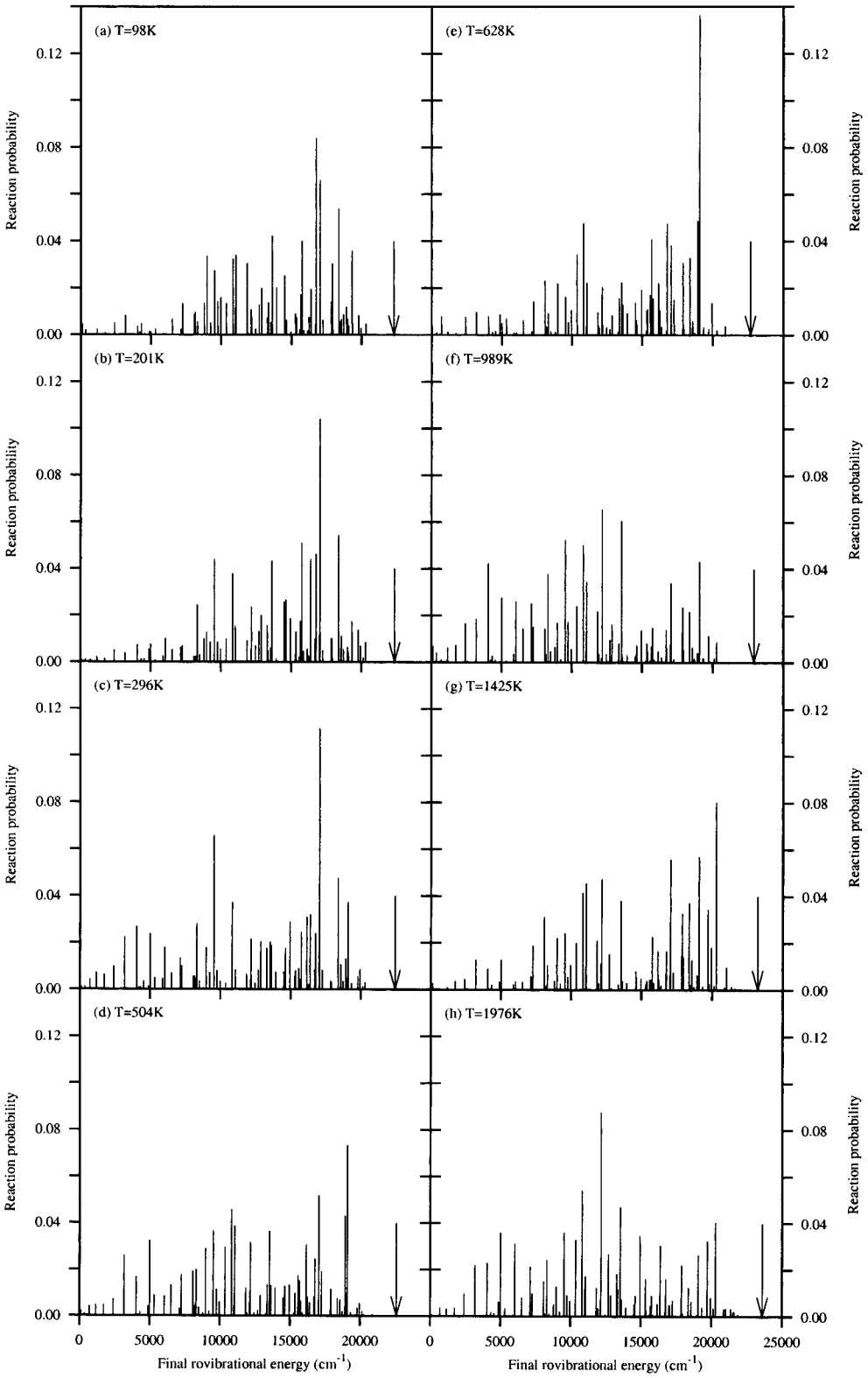

Figure 8. Reaction probabilities for producing H_2 at initial translational energies of the H atom of 98 K, 201 K, 296 K, 504 K, 627 K, 988 K, 1425 K, and 1976 K versus final rovibrational energy of H_2.

and long deBroglie wavelengths. A lower limit of 100 K for the initial translational energy was obtained in this fashion. The 2D calculations in which the H_2 molecule is nonrotating by construction show significant vibrational excitation, with $\nu = 3$ the most abundant.

The 3D calculations show less vibrational excitation. In this case $\nu = 0$ is the most probable vibrational state of the H_2 molecule. Moreover, most molecules have $\nu \leq 2$. Both in the 2D and in the 3D calculations we find that the H_2 molecules are formed with, on average, 40−50% of the total energy as translational energy. This can have important consequences for reaction in the interstellar medium, since the excess translational energy can be used to overcome reaction barriers in endothermic reactions. Moreover, this energy can be transferred to other particles via inelastic collisions, leading to local heating of molecular clouds.

Despite the low level of vibrational excitation, the H_2 molecules are rotationally highly excited with rotational quantum numbers j up to $j = 20$. This could have implications for interstellar chemistry. It also implies that emission from these highly excited states of H_2 could be observed. Our calculations show no preference for the formation of even or odd rotational states (corresponding to p-H_2 and o-H_2, respectively). The rotational distributions for all energies show a bimodal behavior with maxima around $j = 8$ and $j = 14$ and a minimum around $j = 11$. Surface phonons are not included in the present calculations. Given the large effect of the addition of one degree-of-freedom to the quantum mechanical description of the reactive system, corrugation and surface phonons should be included in future calculations to investigate their effect on the reaction probabilities. We also plan to investigate the effect of nonnormal incidence and isotope effects on the reaction probabilities. Jackson et al. found interesting effects in the case of the formation of H_2 on Cu(001)[14] and we expect to find similar effects for the H + H−graphite system.

Acknowledgment. The research was funded by the Particle Physics and Astronomy Research Council, the Engineering and Physical Sciences Research Council, and the Leverhulme Trust. The authors thank the members of the Centre for Cosmic Chemistry and Physics at University College London for helpful discussions.

References and Notes

(1) Rettner, C. T.; Michelsen, H. A.; Auerbach, D. J. *J. Chem. Phys.* **1995**, *102*, 4625.
(2) Rettner, C. T.; Auerbach, D. J.; Tully, J. C.; Kleyn, A. W. *J. Phys. Chem.* **1996**, *100*, 13021.
(3) Hou, H.; Goulding, S. J.; Rettner, C. T.; Wodtke, A. M.; Auerbach, D. J. *Science* **1997**, *277*, 80.
(4) Hodgson, A.; Moryl, J.; Traversaro, P.; Zhao, H. *Nature* **1992**, *356*, 501.
(5) Darling, G. R.; Holloway, S. *Faraday Discuss.* **1998**, *110*, 253.
(6) Dai, J.; Light, J. C. *J. Chem. Phys.* **1998**, *108*, 7816.
(7) Kroes, G.-J.; Baerends, E.-J.; Mowrey, R. C. *Phys. Rev. Lett.* **1997**, *78*, 3583.
(8) Kroes, G.-J. *Prog. Surf. Sci.* **1999**, *60*, 1, and references therein.
(9) Kroes, G.-J.; Baerends, E.-J.; Mowrey, R. C. *J. Chem. Phys.* **1997**, *107*, 3309.
(10) Munn, N. S.; Clary, D. C. *J. Chem. Phys.* **1996**, *105*, 5258.
(11) Kay, M.; Darling, G. R.; Holloway, S. *J. Chem. Phys.* **1998**, *108*, 4614.
(12) Gross, A.; Wilke, S.; Scheffler, M. *Phys. Rev. Lett.* **1995**, *75*, 2718.
(13) Persson, M.; Jackson, B. *J. Chem. Phys.* **1995**, *102*, 1078.
(14) Jackson, B.; Persson, M. *J. Chem. Phys.* **1995**, *103*, 6257.
(15) Caratzoulas, S.; Jackson, B.; Persson, M. *J. Chem. Phys.* **1997**, *107*, 6420.
(16) Kalyanaraman, C.; Lemoine, D.; Jackson, B. *Phys. Chem. Chem. Phys.* **1999**, *1*, 1351.
(17) Shalashilin, D. V.; Jackson, B. *J. Chem. Phys.* **1998**, *109*, 2856.
(18) Shalashilin, D. V.; Jackson, B.; Persson, M. *J. Chem. Phys.* **1999**, *110*, 11038.
(19) Kratzer, P. *J. Chem. Phys.* **1997**, *106*, 6752.
(20) Dai, J.; Light, J. C. *J. Chem. Phys.* **1999**, *110*, 6511.
(21) Weinberg, W. H. *Acc. Chem. Res.* **1996**, *29*, 479.
(22) Burch, R.; Shestov, A. A.; Sullivan, J. A. *J. Catal.* **1999**, *188*, 69.
(23) Kolovos-Vellianitis, D.; Kammler, T.; Küppers, J. *Surf. Sci.* **2000**, *454*−*456*, 316.
(24) Okada, M.; Moritani, K.; Nakamura, M.; Kasai, T.; Murata, Y. *Chem. Phys. Lett.* **2000**, *323*, 586.
(25) Eley, D. D.; Rideal, E. K. *Nature* **1940**, *146*, 401.
(26) Böttcher, A.; Niehus, H.; Schwegmann, S.; Over, H.; Ertl, G. *J. Phys. Chem. B* **1997**, *101*, 11185.
(27) Böttcher, A.; Niehus, H. *Phys. Rev. B* **1999**, *60*, 14396.
(28) Mitchell, W. J.; Xie, J.; Jachimowski, T. A.; Weinberg, W. H. *J. Am. Chem. Soc.* **1995**, *117*, 2606.
(29) Xie, J.; Mitchell, W. J.; Lyons, K. J.; Weinberg, W. H. *J. Chem. Phys.* **1994**, *101*, 9195.
(30) Parneix, P.; Bréchignac, P. *Astron. Astrophys.* **1998**, *334*, 363.
(31) Farebrother, A. J.; Meijer, A. J. H. M.; Clary, D. C.; Fisher, A. J. *Chem. Phys. Lett.* **2000**, *319*, 303.
(32) Gould, R. J.; Salpeter, E. E. *Astrophys. J.* **1963**, *138*, 393.
(33) Hollenbach, D.; Salpeter, E. E. *Astrophys. J.* **1971**, *163*, 155.
(34) Duley, W. W.; Williams, D. A. *Interstellar Chemistry*; Academic Press: London, U.K., 1984.
(35) Barlow, M. J.; Silk, J. *Astrophys. J.* **1976**, *207*, 131.
(36) van der Hulst, H. C. *Rec. Astron. Obs.* **1949**, XI(II).
(37) Hoppe, P.; Zinner, E. *J. Geophys. Res. Space Res.* **2000**, *105*, 10371.
(38) Bernatowicz, T. J.; Cowsik, R.; Gibbons, P. C.; Lodders, K.; Fegley, B., Jr; Amari, S.; Lewis, R. S. *Astrophys. J.* **1996**, *472*, 760.
(39) Messenger, S.; Amari, S.; Gao, X.; Walker, R. M.; Clemett, S. J.; Chillier, X. D. F.; Zare, R. N.; Lewis, R. S. *Astrophys. J.* **1998**, *502*, 284.
(40) Mathis, J. S.; Rumpl, W.; Nordsieck, K. H. *Astrophys. J.* **1977**, *217*, 425.
(41) Fitzpatrick, E. L.; Massa, D. *Astrophys. J. Suppl. Ser.* **1990**, *72*, 163.
(42) Li, A. G.; Greenberg, J. M. *Astron. Astrophys.* **1997**, *323*, 566.
(43) Papoular, R.; Conard, J.; Guillois, O.; Nenner, I.; Reynaud, C.; Rouzaud, J.-N. *Astron. Astrophys.* **1996**, *315*, 222.
(44) Katz, N.; Furman, I.; Biham, O.; Pirronello, V.; Vidali, G. *Astrophys. J.* **1999**, *522*, 305.
(45) Duley, W. W.; Williams, D. A. *Mon. Not. R. Astron. Soc.* **1986**, *223*, 177.
(46) Gough, S.; Schermann, C.; Pichou, F.; Landau, M.; Čadež, I.; Hall, R. I. *Astron. Astrophys.* **1996**, *305*, 687.
(47) Vidali, G.; Pirronello, V.; Liu, C.; Shen, L. *Astrophys. Lett.* **1998**, *35*, 423.
(48) Pirronello, V.; Biham, O.; Liu, C.; Shen, L.; Vidali, G. *Astrophys. J.* **1997**, *483*, L131.
(49) Pirronello, V.; Liu, C.; Roser, J. E.; Vidali, G. *Astron. Astrophys.* **1999**, *344*, 681.
(50) Biham, O.; Furman, I.; Katz, N.; Pirronello, V.; Vidali, G. *Mon. Not. R. Astron. Soc.* **1998**, *296*, 869.
(51) Jeloaica, L.; Sidis, V. *Chem. Phys. Lett.* **1999**, *300*, 157.
(52) Masuda, K.; Takahashi, J.; Mukai, T. *Astron. Astrophys.* **1998**, *330*, 773.
(53) Takahashi, J.; Masuda, K.; Nagaoka, M. *Mon. Not. R. Astron. Soc.* **1999**, *306*, 22.
(54) McCreery, J. H.; Wolken, G., Jr. *J. Chem. Phys.* **1975**, *63*, 2340.
(55) Williams, D. A.; Williams, D. E.; Clary, D. C.; Farebrother, A. J.; Fisher, A. J.; Gingell, J.; Jackman, R.; Mason, N.; Meijer, A. J. H. M.; Perry, J.; Price, S.; Rawlings, J. In *Molecular Hydrogen in Space*; Combes, F., Pineau des Forêts, G., Eds.; Cambridge University Press: Cambridge, U.K., in press.
(56) Colbert, D. T.; Miller, W. H. *J. Chem. Phys.* **1992**, *96*, 1982.
(57) Groenenboom, G. C.; Colbert, D. T. *J. Chem. Phys.* **1993**, *99*, 9681.
(58) Choi, S. E.; Light, J. C. *J. Chem. Phys.* **1989**, *90*, 2593.
(59) Webster, F.; Light, J. C. *J. Chem. Phys.* **1989**, *90*, 265.
(60) Whitnell, R. M.; Light, J. C. *J. Chem. Phys.* **1989**, *89*, 3674.
(61) Hohenberg, P.; Kohn, W. *Phys. Rev.* **1964**, *136*, B864.
(62) Kohn, W.; Sham, L. J. *Phys. Rev.* **1965**, *140*, A1133.
(63) Blöchl, P. E. *Phys. Rev. B* **1994**, *50*, 17953.
(64) Perdew, J. P.; Zunger, A. *Phys. Rev. B* **1981**, *23*, 5048.
(65) Perdew, J. P. *Phys. Rev. B* **1986**, *33*, 8822.
(66) Becke, A. D. *J. Chem. Phys.* **1992**, *96*, 2155.
(67) Waech, T. G.; Bernstein, R. B. *J. Chem. Phys.* **1967**, *46*, 4905.
(68) Huber, K. P.; Herzberg, G. In *Constants of Diatomic Molecules*; (data prepared by J. W. Gallagher and R. D. Johnson, III) in NIST Chemistry WebBook, NIST Standard Reference Database Number 69; Mallard, W. G., Linstrom, P. J., Eds.; National Institute of Standards and Technology: Gaithersburg, MD 20899, 2000; See http://webbook.nist.gov.
(69) Herzberg, G. *Molecular Spectra and Molecular Structure*, Vol. II; van Nostrand: New York, 1945.
(70) Shalashilin, D. V.; Jackson, B.; Persson, M. *Faraday Discuss.* **1998**, *110*, 287.
(71) Schwartz, C. *J. Math. Phys.* **1985**, *26*, 411.
(72) Goldfield, E. M.; Meijer, A. J. H. M. *J. Chem. Phys.*, accepted.
(73) Gray, S. K.; Balint-Kurti, G. G. *J. Chem. Phys.* **1998**, *108*, 950.
(74) Huang, Y.; Iyengar, S. S.; Kouri, D. J.; Hoffman, D. K. *J. Chem. Phys.* **1996**, *105*, 927.
(75) Mandelshtam, V. A.; Taylor, H. S. *J. Chem. Phys.* **1995**, *103*, 2903.
(76) Kroes, G.-J.; Neuhauser, D. *J. Chem. Phys.* **1996**, *105*, 8690.
(77) Chen, R.; Guo, H. *J. Chem. Phys.* **1996**, *105*, 3569.
(78) Meijer, A. J. H. M.; Goldfield, E. M.; Gray, S.; Balint-Kurti, G. G. *Chem. Phys. Lett.* **1998**, *293*, 270.
(79) Meijer, A. J. H. M.; Goldfield, E. M. *J. Chem. Phys.* **1998**, *108*, 5404.
(80) Gray, S. K.; Wozny, C. E. *J. Chem. Phys.* **1989**, *91*, 7671.
(81) Zhang, D. H.; Zhang, J. Z. H. *J. Chem. Phys.* **1994**, *101*, 3671.
(82) Zhang, J. Z. H. *Theory and Application of Quantum Molecular Dynamics*; World Scientific: Singapore, 1999.